Origins of tropospheric ozone interannual variation (IAV) over Réunion: A model investigation

Junhua Liu[1,2,*], Jose M. Rodriguez[2], Anne M. Thompson[2], Jennifer A. Logan[3], Anne R. Douglass[2], Mark A. Olsen[2,4], Stephen D. Steenrod[1,2] , Francoise Posny[5]

[1] Universities Space Research Association (USRA), GESTAR, Columbia, MD, USA

[2] NASA Goddard Space Flight Center, Greenbelt, Maryland, USA

[3] School of Engineering and Applied Sciences, Harvard University, Cambridge, MA, USA

[4] Morgan State University, Baltimore, MD, USA

[5] Laboratoire de l'Atmosphère et des Cyclones (LACy), Université de La Réunion/CNRS, La Réunion, France

*Corresponding author's email address: junhua.liu@nasa.gov

Key Points

1: The GMI-CTM Model simulated the main features of the observed ozone IAV over Réunion.

2: Stratospheric input plays an important role in the tropospheric ozone IAV over Réunion.

3: Changes in emissions have little influence on middle and upper tropospheric ozone over Réunion.

Abstract

Observations from long-term ozonesonde measurements show robust variations and trends in the evolution of ozone in the middle and upper troposphere over Réunion Island (21.1°S, 55.5°E) in June-August. Here we examine possible causes of the observed ozone variation at Réunion Island using hindcast simulations by the stratosphere-troposphere Global Modeling Initiative chemical transport model (GMI-CTM) for 1992-2014, driven by assimilated Modern-Era Retrospective Analysis for Research and Applications (MERRA) meteorological fields. Réunion Island is at the edge of the subtropical jet, a region of strong stratospheric-tropospheric exchange (STE). Our analysis implies that the large interannual variation (IAV) of upper tropospheric ozone over Réunion is driven by the large IAV of the stratospheric influence. The IAV of the large-scale, quasi-horizontal wind patterns also contributes to the IAV of ozone in the upper troposphere. Comparison to a simulation with constant emissions indicates that increasing emissions do not lead to the maximum trend in the middle and upper troposphere over Réunion during austral winter implied by the sonde data. The effects of increasing emission over southern Africa are limited to the lower troposphere near the surface in August - September.

1. Introduction

Tropospheric ozone plays an important role in the oxidative capacity of the troposphere and in atmospheric radiative forcing [e.g., *Lacis et al.*, 1990; *Fiore et al.*, 2002; *Forster et al.*, 2007; *Sitch et al.*, 2007; *Stevenson et al.*, 2013]. It acts as a direct greenhouse gas in the upper troposphere and lower stratosphere (UTLS) and has contributed significantly to climate change. It also impacts the air quality near the

47 surface, with harmful effects on human health and crop yields [e.g., *Bell et al.*, 2005;
48 *Silva et al.*, 2013]. Ozone is produced in the troposphere by photochemical oxidation of
49 CO and volatile organic compounds (VOCs) in the presence of nitrogen oxides (NO_X)
50 [e.g., *Logan et al.*, 1981]. These ozone precursors are emitted both from anthropogenic
51 sources, including fossil fuel combustion and biomass burning, and from natural sources
52 such as lightning. Moreover, in regions of subsidence, tropospheric ozone may be
53 significantly affected by ozone input from the stratosphere. Long-range transport, most
54 significant in the middle and upper troposphere where the ozone lifetime is several weeks
55 [*Fusco and Logan*, 2003], also contributes to the tropospheric ozone distribution [*Sudo*
56 *and Akimoto*, 2007].

57 A recent study by Thompson et al. [2014] identified a significant increase in
58 tropospheric ozone at Réunion (21°S, 55°E) in June-July-August (JJA) from 1992 to
59 2011 based on ozonesonde measurements. The observed increase is up to 50%/decade in
60 the upper troposphere. This result extended the study by Clain et al. [2009], who found a
61 strong positive ozone trend in the middle and upper troposphere in JJA based on Réunion
62 sondes for 1992 to 2008. The sonde data also show large interannual variability (IAV),
63 which complicates the estimation and diagnosis of trends. In this study, we use the
64 stratosphere-troposphere Global Modeling Initiative chemical transport model (GMI-
65 CTM) model to interpret the observed IAV and trends of tropospheric ozone over
66 Réunion from 1992 to the present. In so doing, we investigate the impact of stratospheric
67 input and surface emissions during the past 20 years.

68 Earlier studies have used tropospheric CTMs to examine the response of
69 tropospheric ozone to changes in stratospheric input and in surface emissions; these

models used a simple treatment of stratospheric influence, in which they used either the SYNOZ (synthetic ozone) approach developed by McLinden et al. [2000] of specifying the flux [e.g., the GEOS-Chem model in *Fusco and Logan*, 2003; *Hess and Zbinden*, 2013], or they specified ozone in the lower stratosphere [*Karlsdottir et al.*, 2000; the GISS model in *Fusco and Logan*, 2003]. Pozzoli et al. [2011] simulated tropospheric composition for 1980-2005 using an aerosol-chemistry climate model driven by the European Centre for Medium-Range Weather Forecasts (ECMWF) 40-year reanalysis (ERA-40) data and operational analyses. The two simulations with constant and varying anthropogenic emissions show similar IAV in surface ozone, suggesting that changes in meteorology and natural emissions contribute greatly to the ozone IAV, which may mask contrasting regional trends driven by anthropogenic emissions in surface ozone in any given period. Lin et al. [2014] argued that shifts in atmospheric circulation patterns contribute to the observed tropospheric ozone trends at Mauna Loa, the western US, and the northern mid-latitudes in recent decades based on a suite of chemistry–climate model simulations. Hess et al. [2015] analyzed the effects of stratospheric input to tropospheric ozone variations over the northern hemisphere mid-latitudes with four ensemble simulations of the free running Whole Atmosphere Community Climate Model (WACCM) for 1953 to 2005. Their model used a standard stratospheric chemical mechanism, but with simple CH_4-NO_X chemistry in the troposphere with constant surface chemical emissions. The agreement of the simulated and observed tropospheric ozone IAV in Hess et al. (2015) suggests that natural variability plays a big role controlling the IAV of tropospheric ozone over the northern hemisphere (NH). Most of these studies focused on the northern hemispheric extra-tropics. Far fewer studies have focused on the

93 long-term behavior of ozone in southern hemisphere (SH) owing to a lack of suitable
94 observations.

95 In our study, taking advantage of the multi-year record from Réunion sondes and
96 hindcast simulations from the GMI-CTM model [*Duncan et al.*, 2007; *Strahan et al.*,
97 2007], we investigate the causes of observed interannual and decadal variations of
98 tropospheric ozone over Réunion. Our analysis is based on a series of hindcast
99 simulations for 1992-2014 with the GMI-CTM driven by assimilated Modern-Era
100 Retrospective Analysis for Research and Applications (MERRA) meteorological fields
101 [*Rienecker et al.*, 2011]; the GMI-CTM includes a comprehensive stratospheric and
102 tropospheric chemical mechanism. The simulations include a stratospheric ozone tracer
103 to examine the stratospheric contribution. We also use a control simulation with constant
104 emissions to explore the influence from surface emissions.

105 Réunion Island (20.8°S, 55.5°E) is in the western part of the south Indian Ocean,
106 about 1000 km east of Madagascar. In the upper troposphere, the position of Réunion is
107 near the boundary between tropical air with low ozone and the subtropical jet region with
108 high ozone (Figure 1 in Thompson et al. 2014). The dominant meteorological features in
109 the troposphere over Réunion are subject to competition between tropical and subtropical
110 influences on the general circulation. The meteorology is also affected by the
111 perturbations from the South Indian Ocean anticyclone and wave propagation in the
112 westerlies [*Waugh and Polvani*, 2000; *Randriambelo et al.*, 2003]. Observations and
113 meteorological data show that tropospheric ozone variations over this region are mainly
114 influenced by stratospheric intrusions through various dynamical mechanisms [*Baray et*
115 *al.*, 1998; *Postel and Hitchman*, 1999; *Baray et al.*, 2003; *De Bellevue et al.*, 2007; *Clain*

116 *et al.*, 2009]. Škerlak et al. [2014] extracted a global climatology of stratosphere–
117 troposphere exchange (STE) using the ERA-Interim data set from 1979 to 2011. Their
118 results show a large latitudinal gradient in the ozone flux from stratosphere to
119 troposphere to the south of Réunion in JJA as well as other seasons. Tropospheric ozone
120 at Réunion shows a strong seasonal cycle with an austral winter-spring maximum and
121 summer minimum [*Baldy et al.*, 1996; *Taupin et al.*, 1999; *Randriambelo et al.*, 2000].
122 The summer minimum is due to a combination of photochemical loss and inflow of
123 tropical marine air with the development of deep convection [*Taupin et al.*, 1999; *Clain*
124 *et al.*, 2009]. The winter-spring maximum has been attributed by several previous studies
125 to a combined influence of surface emission and stratospheric influence [e.g., *Taupin et*
126 *al.*, 1999; *Randriambelo et al.*, 2000; *Thompson et al.*, 1996; 2003].

127 Réunion is located downwind of emissions from southern Africa and Madagascar.
128 Several studies based on trajectory statistics suggested that a portion of African emissions
129 might be transported to the Indian Ocean [*Garstang et al.*, 1996; *Piketh et al.*, 2002; *Sudo*
130 *and Akimoto*, 2007; *Thompson et al.*, 2014]. Southern Africa, one of the major biomass-
131 burning regions in the southern hemisphere, also has an abundance of industrial and other
132 anthropogenic sources. Lelieveld et al. [2004] found that anthropogenic NO_X emissions
133 doubled from 1977 to 2001 (0.8 to 1.6 Tg/year) over Africa based on a historical
134 emission inventory. Sauvage et al. [2007] showed that emissions over the Eastern regions
135 (India, South-East Asia, Australia) have a broad influence throughout the Pacific and
136 Indian Oceans, with the maximum contribution for ozone changes over Réunion region in
137 JJA. They argued that the Eastern source emissions were transported to the upper level
138 anticyclone associated with the Indian monsoon system [*Hoskins and Rodwell*, 1995;

139 *Rodwell and Hoskins*, 2001], then trapped in the Tropical Easterly Jet, which peaks in
140 JJA [*Hastenrath and Wu*, 1982], and transported cross-equator to North Africa, the
141 Atlantic and Indian ocean. The changes in anthropogenic emissions from the Eastern
142 region may also contribute to the observed positive trends at Réunion. We will examine
143 the effects of changes of emissions using a sensitivity simulation with constant emissions,
144 including emissions from biomass burning, fossil fuel and biofuel burning, in section 3.3.
145 Section 2 provides an overview of the GMI-CTM simulations and the ozonesonde
146 measurements. Section 3.1 evaluates the vertical and spatial distribution of tropospheric
147 ozone in the model using ozonesonde data and GMAO assimilated data. Section 3.2
148 presents a diagnostic study of factors controlling the observed ozone IAV in the upper
149 troposphere at Réunion using GMI-CTM model simulations. Section 3.3 focuses on the
150 trends in observed and model simulated tropospheric ozone. Conclusions and the
151 discussion of the dynamical effects on tropospheric ozone IAV are described in section 4.

152 **2. Measurements and Model**

153 **2.1. GMI CTM hindcast simulations**

154 We used the GMI CTM [*Duncan et al.*, 2007; *Strahan et al.*, 2007] driven by
155 MERRA reanalysis meteorology [*Rienecker et al.*, 2011, http://
156 gmao.gsfc.nasa.gov/research/merra/]. MERRA was produced with the NASA Goddard
157 Earth Observing System (GEOS) version 5.2.0 data assimilation system with the native
158 horizontal resolution of $0.67° \times 0.5°$ and 72 vertical levels. The vertical resolution of
159 MERRA fields is ~ 1km in the upper troposphere and lower stratosphere. We regrid to
160 2°x2.5° for input to the base GMI-CTM simulations. MERRA uses a modified version of
161 the Relaxed Arakawa-Schubert convective scheme (RAS) described by Moorthi and

Suarez [1992]. The model reads in the planetary boundary layer (PBL) from MERRA and follows the full mixing scheme where emissions and concentrations of individual species are evenly distributed in the PBL. The model includes a complete treatment of stratospheric and tropospheric chemistry coupled with aerosol mechanism derived from the GOCART model [*Chin et al.*, 2002]. Biogenic emissions of isoprene and monoterpenes follow the latest version of the MEGAN algorithm [*Guenther et al.*, 2006]. Biomass burning emissions are from the Global Fire Emission Database, GFED3 [van der Werf et al., 2010]. Emission before 1997 are retrieved from GFED3 emission climatology averaged for 2001 to 2009 with regional-scale IAV applied, which was derived from satellite information on fire activity (ATSR) and/or aerosol optical depths from the Total Ozone Mapping Spectrometer (TOMS) by Duncan et al. [2003]. Anthropogenic emissions are based on the EDGAR 3.2 Inventory [*Olivier et al.*, 2005], overwritten with the regional inventories for North America, Europe, and Asia. More details are given in Strode et al. (2015). Emission data were only available through year 2011 when our hindcast simulations were conducted. Consequently, we repeat the emissions of year 2011 for years of 2012-2014. The lightning NO_X is calculated online following the scheme described by Allen et al. (2010). The global total of NO_x from lightning is set the same of 5.00 Tg N/yr every year in the hindcast. Methane mixing ratios are specified in the two lowest model levels, using time dependent zonal means from NOAA/GMD. Other long-lived source gases important in the stratosphere, such as N_2O, CFCs and halocarbons are forced monthly at the two lowest model levels based on the A2 scenario as described in Strahan et al. [2007]. Stratospheric aerosol distributions/trends are from IGAC/SPARC and have IAV [*Stolarski et al.*, 2006].

185 Our standard simulation (labeled as Hindcast-VE) used in this study for 1992-
186 2014 includes monthly and inter-annually varying emissions of fossil fuel, biomass
187 burning and biofuel. We carry out a control run with constant emissions fixed at year
188 2000 levels, which is labeled as Hindcast-CE. We also conduct a high-resolution
189 simulation (labeled as Hindcast-VE-HR) at 1.25°x1° horizontal resolution to explore the
190 effect of model's horizontal resolution on ozone simulation.

191 The model includes a stratospheric ozone tracer ($StratO_3$). The $StratO_3$ is defined
192 relative to a dynamically varying tropopause tracer (e90) [*Prather et al.*, 2011], which
193 has been implemented in the GMI model. The e90 tracer is an artificial tracer emitted at
194 the surface uniformly (100 ppb) with a 90-day e-folding lifetime. In our simulation, the
195 e90 tropopause value is 90 ppb. The StratO3 tracer is set equal to ozone in the
196 stratosphere and is removed in the troposphere with the loss frequency (chemistry and
197 deposition) archived from daily output of Hindcast-VE simulation in this study. There is
198 no production of $StratO_3$ in the troposphere. Using the $StratO_3$ tracer allows quantification
199 of ozone of stratospheric origin in the troposphere at a given location and time. This
200 approach has also been adopted in the high resolution GFDL AM3 model [*Lin et al.*,
201 2012].

202 **2.2. Réunion ozone sonde measurements**

203 Vertical ozone profiles were measured since September 1992 at Réunion Island
204 from radiosondes using three manufacturers (Science Pump Corporation: SPC, EN-SCI
205 Corporation: ENSCI-Z and ENSCI-Droplet Measurement Technologies: ENSCI-DMT)
206 [*Baldy et al.*, 1996; *Baray et al.*, 2006; *Thompson et al.*, 2014]. Although these changes
207 are not recorded in the SHADOZ metadata (http://croc.gsfc.nasa.gov/shadoz/), the

208 lacking of instrument uniformity could have minor impacts on calculated trends. Overall
209 sonde data quality assurance during SHADOZ's period (1998-2014) can be inferred
210 from comparisons between sonde total ozone at Réunion and TOMS (to 2005) and OMI
211 (after 2005) overpass, as well as Systéme d'Analyse par Observation Zénitale (SAOZ)
212 [Thompson et al., 2003; 2007; 2012], which do not show evidence of systematic
213 instrumental change. The ozone measurements are on a bi-weekly/monthly basis. A
214 standard meteorological radiosonde is attached to the ozonesondes to simultaneously
215 transmit the profiles of atmospheric temperature, pressure, and humidity, along with the
216 ozone data: Vaisala RS80 (prior to Sept 2007) then Modem M2K2 and M10 (since April
217 2013). The Modem sondes measure in addition the position, the wind speed and direction
218 (Doppler GPS). Thompson et al. [2012] showed that the column ozone over Réunion for
219 2005-2009 as measured by the sondes was within 2-3% of OMI satellite measurements
220 and the measurements of SAOZ instrument, co-located at Réunion Island.

221 To compare GMI-CTM model output with the Réunion sonde profiles, we extract
222 the model grid box containing Réunion Island and sample the model profiles on the date
223 of each observation. The Réunion ozonesondes provide high-vertical-resolution profiles
224 of ozone (~100m) through the depth of the troposphere. We convert the sonde profiles
225 from high-resolution to the low-resolution vertical grid used in model. In our algorithm,
226 we integrate the high-resolution sonde profiles at their pressure levels to get the
227 accumulated partial column ozone profiles in Dobson Units (DU). We then interpolate
228 the integrated profiles into the MERRA reduced vertical grid with 47 fixed pressure
229 levels and convert them back to mixing ratio in ppbv following the method as described
230 in Ziemke et al. [2001].

231 **2.3. GMAO assimilated ozone data**

232 We also used assimilated tropospheric ozone to evaluate overall model
233 performance. This assimilated dataset is produced by ingesting OMI v8.5 total column
234 ozone and MLS v3.3 ozone profiles into a version of the Goddard Earth Observing
235 System, Version 5 (GEOS-5) data assimilation system [*Rienecker et al.*, 2011]. No
236 ozonesonde data are used in the assimilation. Wargan et al. [2015] provides details of the
237 GEOS-5.7.2 assimilation system, which for this application is run with a horizontal
238 resolution of 2° latitude by 2.5° longitude and with 72 vertical layers between the surface
239 and 0.01 hPa. For the troposphere, the assimilation applies only a dry deposition
240 mechanism at the surface without any chemical production or loss. This algorithm works
241 since the ozone lifetime is much longer than the six-hour analysis timesteps. Ziemke et al.
242 [2014] evaluated the tropospheric ozone profiles derived from OMI and MLS
243 measurements using three strategies to quantify the tropospheric ozone column (this
244 GEOS-5 assimilation, trajectory mapping and direct profile retrieval using the residual
245 method) with ozonesonde observations and GMI model simulations. They found that the
246 tropospheric ozone product from the GEOS-5 assimilation is the most realistic one.
247 Wargan et al. [2015] also demonstrate that the upper tropospheric ozone (500 hPa to the
248 tropopause) from GEOS-5 assimilation is in good agreement with independent
249 observations from ozonesondes. Therefore, we treat the ozone from the GEOS-5
250 assimilation as a reference value and use it to evaluate our GMI model simulation. We
251 use partial column ozone integrated from 500 hPa to the tropopause from the GEOS-5
252 assimilation, because there is no direct observational constraint in the analysis in the
253 lower troposphere (the OMI kernels have no weight in the lowest layers) and the

254 assimilation system does not account for chemical production by fast chemical processes,
255 such as NO_X emissions [*Wargan et al.*, 2015]. We use the same tropopause as defined by
256 the lowest of the 3.5 PVU/380K control surface to calculate the tropospheric ozone
257 column.

258 **3. Results**

259 **3.1. Ozone profile and model evaluation**

260 The temporal evolution of observed ozone vertical profiles from Réunion
261 ozonesondes in July and August from 1992 to 2014 is shown in Fig. 1. The ozone
262 concentration in the middle and upper troposphere stayed low in the early 1990s then
263 increased continuously around year 2000 in both July and August. The profiles in 1990s
264 have steep ozone gradients in the upper troposphere and lower stratosphere, and a
265 relatively uniform and low ozone layer in the middle and lower troposphere. The profiles
266 in 2000s show greater IAV and occasionally have large increases of ozone in the middle
267 and upper troposphere (e.g., July 2006, 2011; August 2006, 2008, 2010, 2013).
268 Evidently, the occurrence of these ozone maxima in the 2000s are the main reason for the
269 positive ozone trends in July and August calculated by Thompson et al. (2014) over
270 Réunion.

271 A recent study by Lin et al. [2015] concluded that the weekly ozone sonde
272 measurements at Trinidad Head and Boulder do not faithfully capture the actual
273 variability of mean mid-tropospheric ozone due to the sparse sample frequency. The
274 issue of the sampling frequency of sondes (weekly or sparser at many sites) has also been
275 raised by many previous studies, often in the context of tropospheric trends [e.g., *Cooper*
276 *et al.*, 2010; *Logan et al.*, 2012], but also in terms of climatology [*Logan*, 1999], and in

277 terms of different types of variability, including interannual [e.g., *Logan et al.*, 2012;
278 *Saunois et al.*, 2012]. We therefore used model simulations to check the adequacy of the
279 sampling frequency over Réunion. Figure 2 compares simulated monthly mean ozone
280 mixing ratio at 226 hPa, 313 hPa, and 510 hPa averaged from the GMI-CTM Hindcast-
281 VE-HR run (1°x1.25°, with varying emissions) co-sampled with the available sonde
282 observations (red lines), and the monthly mean of the model daily output (green lines)
283 from 1992 to 2014. The phases of interannual variations are often similar between the
284 two monthly means, with some obvious discrepancies particularly in the upper
285 troposphere. The variations in the co-sampled means tend to have a larger magnitude.
286 This is not unexpected, as Réunion is located in a both dynamically and chemically active
287 region with a large ozone gradient, and the sampling is infrequent. The agreement of
288 monthly means between these two sampling methods is better at 510 hPa than at upper
289 levels. We also compare the monthly mean from daily output and the means determined
290 with different sampling frequencies (e.g., monthly, bi-weekly, weekly). The results
291 suggest that increasing sampling frequency to 4 per month would be enough to reproduce
292 the IAV of the mean from daily output. Although the current sparse sampling cannot fully
293 reproduce the IAV in the monthly means of daily output in the upper troposphere, we can
294 evaluate how well the model captures the variability that is revealed by the sonde
295 data by co-sampling the model on the dates of the soundings, and then use the
296 model to examine mechanisms influencing the IAV.

297 Unlike the IAV, the derived trends are very sensitive to the sampling
298 frequency, as well as other factors, such as years used in the trend calculation (see
299 below). In July, the mean of daily output shows statistically significant positive trends

300 both at 226 hPa and 313 hPa. These trends become insignificant when sampled at the
301 ozonesonde measurement time. In August, the significant positive trends in 'sampled'
302 monthly mean become insignificant in the monthly mean ozone of daily output at 226
303 hPa and 313 hPa. Given the limitations of the sampling as well as other factors
304 affecting calculated trends, we have not focused on the trends at Reunion, except for
305 an analysis of the influence of trends in emissions.

306 Figure 3 compares the modeled and observed tropospheric ozone at Réunion
307 averaged over 1992-2002 and 2003-2014 from the upper to the lower troposphere. The
308 observed monthly mean ozone is generally higher (~10-20 ppb) in the upper troposphere
309 during the most recent period compared to the previous period. The difference between
310 these two periods is smaller in both model simulations. At 226 hPa, the Hindcast-VE
311 simulation (red) agrees very well with the observed phase of the annual cycles during
312 both periods, but is too high by 10-15 ppb for 1992-2002. From 313 hPa to 694 hPa, the
313 Hindcast-VE simulations overestimate the observations from June to August over both
314 periods. The overestimates are largest (~12 ppb) in the upper troposphere and decrease to
315 ~5 ppb in the middle and lower troposphere. Ozone from the high-resolution simulation
316 (blue) is systematically lower than that from the low-resolution simulation by an average
317 of 15 ppb in the upper troposphere and less than 5 ppb in the lower troposphere, resulting
318 in a better agreement with observations in June to August from 313 hPa to 694 hPa. At
319 226 hPa, the high-resolution simulation reduces the overestimate as seen in the low-
320 resolution simulation for 1992-2002, but underestimates the observations for 2003-2014.

321 Figure 4 shows the spatial pattern of southern hemispheric ozone partial columns
322 in the upper troposphere (integrated from 500 hPa to the tropopause) averaged over 2005

323 to 2012, when GMAO assimilated data are available, for the four seasons from the
324 GMAO assimilated dataset based on OMI/MLS (left column) and the GMI hindcast-VE
325 simulation (middle column) and their absolute difference (right column). Wargan et al.
326 (2015) argue that the UT ozone column (from 500 hPa to the tropopause) within 30°S-
327 30°N latitude bands has a low bias of 2.5 ± 3.8 DU compared to sonde measurement. We
328 therefore adjusted the GMAO assimilated ozone by adding 2.5 DU to compare to the
329 GMI hindcast simulation. Both show the wave one ozone maximum, a predominantly
330 Southern Hemisphere phenomena, with ozone maximum localized in the southern
331 Atlantic - southern Africa - western Indian Ocean region [*Logan and Kirchhoff*, 1986;
332 *Thompson et al.*, 1996; 2003; *Sauvage et al.*, 2006; 2007]. Over these ozone maximum
333 regions, although the GMI hindcast simulations are too high compared to the assimilated
334 ozone, most of the model overestimations are within the bias range as suggested by
335 Wargan et al. [2015]. In general, the GMI hindcast simulation reproduces the seasonality
336 and spatial distribution of the upper tropospheric column ozone from the assimilated
337 product.

338 **3.2. IAV**

339 Figure 5 shows the temporal variation of observed (black) and simulated ozone
340 (red) and the simulated $StratO_3/O_3$ ratio (blue) at 313 hPa in July and August from 1992
341 to 2014. The monthly mean simulations are calculated from daily output sampled on the
342 date of sonde measurements. In July, sonde and model agree well on the IAV of O_3 at
343 313 hPa ($r = 0.78$, $P < 0.001$) and are similar to the phase of the IAV of the $StratO_3/O_3$
344 ratio. For example, both sonde and model show an ozone minimum in 1997, 2004, and
345 2011 when the stratospheric ozone contribution inferred from the $StratO_3/O_3$ ratio reaches

346 a minimum. In July 1998, 2006 and 2012, both sonde and model show an ozone
347 maximum, concurrent with the maximum in the $StratO_3/O_3$ ratio. In August, a similar but
348 somewhat weaker coupling is observed between ozone mixing ratio and $StratO_3/O_3$ ratio
349 at 313 hPa. The IAV of both the simulated ozone and $StratO_3/O_3$ ratio is relatively
350 constant through the two decades, while the IAV in observed ozone is relatively small
351 during the first decade compared to that in the second decade (Figure 5). Therefore, the
352 IAV of simulated ozone shows a better agreement with the IAV of sonde observations in
353 the 2000s. An independent initial analysis of total column ozone based on satellite and a
354 MERRA-forced GMI-CTM simulation also suggests better agreements after year 2000
355 (L. D. Oman, personal communication, 2015), when many more higher resolution
356 meteorological observations are included in the MERRA assimilation [*Rienecker et al.*,
357 2011]. Nevertheless, the model captures many of the observed peaks and troughs in the
358 sonde measurements. The good agreement between tropospheric ozone IAV with that of
359 $StratO_3/O_3$ ratio during austral winter indicates that changes in the stratospheric ozone
360 contribution play an important role in the observed IAV in winter over Réunion at 313
361 hPa, particularly in July when $StratO_3$ explains about 44% of the model variance.
362 Figure 6 shows a similar plot in December, when both STE and surface emissions
363 over southern Africa reach their seasonal minimum. The model agrees well with the
364 observed ozone from sondes in the upper troposphere ($r = 0.64$, $P< 0.005$). It matches the
365 magnitudes and phase changes of observed IAV, except for 2005, 2012-2013. The
366 stratospheric ozone contribution explains about ~27% of the variance of model ozone,
367 which indicates even in austral summer the IAV of stratospheric input contributes to IAV
368 of upper tropospheric ozone over Réunion.

369 To diagnose and examine the impact of stratospheric input and other dynamical
370 mechanisms on the tropospheric ozone at the interannual time scale, we selected July
371 1997 and 2006 as two extreme examples. The top two panels of Figure 7 show the spatial
372 maps of simulated ozone mixing ratio at 313 hPa in July 1997 and 2006. Both years show
373 a similar ozone spatial pattern. Ozone reaches a minimum over Indonesia, which is
374 caused by strong convection over this region [*e.g., Logan et al.,* 2008]. The very high
375 ozone is widespread across the southern Atlantic, southern Africa, southern Indian Ocean
376 region and western Pacific, centered at 30°S where the subtropical jet is located. The
377 black cross denotes the location of Réunion, with steep gradients in ozone. It is clearly
378 seen from Figure 7 that in July 1997, Réunion is located at the edge of the ozone
379 maximum zone, while in July 2006, Réunion is in its center. The difference in ozone over
380 Réunion at 313 hPa is up to 20 ppb (~30%) between these two years. The bottom two
381 panels show the spatial maps of the corresponding $Strat O_3/O_3$ ratio, which represent the
382 influence of stratospheric air on tropospheric ozone. The stratospheric influence shows a
383 minimum over the tropics and maximum contribution over the subtropics, which is
384 closely related to the Brewer Dobson circulation [*Brewer*, 1949; *Dobson*, 1956; *Holton et*
385 *al.*, 1995]. Réunion is located right on the boundary of the tropical convection regions
386 and the subtropical jet system with a sharp gradient in the stratospheric input. In July
387 1997, the equatorward boundary of regions with strong stratospheric influence moves
388 southward and Réunion falls out of this region. In July 2006 Réunion falls in the region
389 with strong stratospheric influence, resulting in the ozone maximum. Evidently the large
390 interannual differences in the stratospheric contribution of ozone cause the strong IAV of
391 tropospheric ozone over Réunion. Ozone is most abundant over the regions where

392 stratospheric influences are highest.

393 Figure 8 shows the profiles of observed (black) and the simulated ozone from
394 GMI-CTM Hindcast-VE (red) and GMI-CTM Hindcast-VE-HR (blue) in July 1997 and
395 2006 at Réunion. In July 1997, ozone concentrations are low (~30 ppb) through the
396 troposphere and are representative of major influence from tropical marine air. In July
397 2006, the ozone concentration slowly increases with altitude, with an ozone peak up to 90
398 ppb in the upper troposphere both in measurements and model simulations, reflecting the
399 contributions from stratospheric high ozone air. Ozone profiles from both simulations
400 reproduce the shape of observed ozone profile in July 1997, but the models are too high
401 in the middle and upper troposphere by ~10 ppb. In July 2006, the ozone profile from
402 high-resolution simulation agrees very well with the observed ozone profile below 300
403 hPa, while results from the low-resolution run are too high.

404 We also examined the influence of the prevailing horizontal transport on the IAV
405 of tropospheric ozone near Réunion. Figure 9 shows the monthly mean ozone mixing
406 ratio superimposed on the spatial wind pattern at 313 hPa in July 1997 and 2006. In July
407 1997, northwesterly winds prevail over Réunion Island, and bring in tropical low ozone
408 air. In July 2006, the southerly winds encroach from the south and converge near
409 Réunion Island, which bring in mid-latitude high ozone air, with the strongest $StratO_3$
410 contribution (Figure 7). The combined contributions from horizontal and vertical
411 dynamics result in the ozone maximum in 2006 at Réunion. The IAV of large-scale wind
412 patterns reinforce the changes in the stratospheric contribution and contribute to IAV of
413 upper tropospheric ozone.

414 **3.3. Trends**

Figure 10 shows the trend profiles as a function of month for the observations and model simulation (Hindcast-VE) at Réunion from 1992 to 2014 in units of ppb/decade. The trends are calculated from a linear regression trend model that includes factors of the seasonal cycle and trends as discussed by Ziemke et al. [1997]. The black lines indicate statistical significance at 90% confidence interval. Similar profiles of trends calculated from the ozonesondes but for 1992-2011 (as in Thompson et al. 2014) are shown in Fig. S1. The trend maximum in JJA in the middle and upper troposphere calculated for 1992-2014 is about 19 ppb/decade at 164 hPa (Fig. 10a), which is ~ 5 ppb/decade lower than the trend maximum for 1992-2011, showing the sensitivity of the trend to the selected period. The model simulations reproduce the key features and general morphology of observed trends, but underestimate the maximum trend in the sonde data in July-August in the middle and upper troposphere by ~ 6 ppb/decade (Hindcast-VE, Fig. 10b). The model co-sampled with the available sonde observations also shows statistically significant positive trends between 200 and 400 hPa in November-December, in agreement with the observed secondary maximum (Fig. 10a).

3.4. Sensitivity to time-dependent emissions

Figure 11 shows the temporal variation of total NO emissions and NO emissions from fossil fuel and biomass burning in our model in July - September from 1992 to 2011 over southern Africa and Eastern regions. In southern Africa, the NO emissions are mainly driven by the IAV of biomass burning. Both fossil fuel and biomass burning emissions show a slightly positive trend in July-September. In the Eastern region, the trend of NO emission is mainly driven by the fossil fuel combustions, and biomass burning contributes to the IAV. For example, the 1997 peak in NO emissions over the

438 Eastern region was driven by the record-setting forest fires in Indonesia. The fossil fuel
439 emissions from the Eastern region show a substantial increase over 20 years, which could
440 contribute to the observed positive trends at Réunion through the pathway described
441 earlier. We examined the effects of varied emission on tropospheric ozone over Réunion
442 using a sensitivity run with constant emissions. Figure 12 shows the calculated ozone
443 trend from 1992 to 2011, the period that the Hindcast-VE has the yearly-varied emissions
444 input, between runs with varied emission and constant emission (Hindcast-VE and
445 Hindcast-CE). It shows that differences of simulated ozone trends between these two runs
446 are quite small (<1ppb/decade). The maximum increases due to emission changes occur
447 in the upper troposphere from July to September and near the surface from August and
448 September. The increase in the upper troposphere is probably caused by the cross-equator
449 transport of increased emissions from the Eastern region in the upper troposphere. The
450 near-surface ozone increase in August-September possibly results from increased
451 emissions over southern Africa and Madagascar. Senten et al., [2008] confirmed the
452 impacts from burning events in Africa and Madagascar on the tropospheric chemical
453 composition over Reunion based on an event study in October 2004, using the
454 measurements from ground-based high spectral resolution Fourier-transform infrared
455 (FTIR) solar absorption spectroscopy campaign and the FLEXPART simulation. The
456 results in Figure 12 imply that the increase due to emission only accounts for ~15% of the
457 ozone change and does not explain the observed trend maximum in the middle and upper
458 troposphere over Réunion during austral winter.

459 **4. Summary and Discussion**

460 In this study we used the GMI-CTM model to interpret the trend and interannual

461 variations of tropospheric ozone recorded by ozonesondes from 1991 to 2014 over
462 Réunion. Comparisons of the observations and simulations, along with an analysis of the
463 MERRA meteorology, the influence of surface emissions, and of stratospheric
464 contributions using the $StratO_3$ tracer, provide an understanding of factors controlling the
465 temporal variations of tropospheric ozone at this location. Our analysis also reveals
466 limitations of low-resolution model simulations, as well as successes. It also implies that
467 the bimonthly/monthly sonde measurements at Reunion are too sparse to give reliable
468 trend estimates.

469 The model reproduces 61% of the observed interannual variance of tropospheric
470 ozone over Réunion in July, and less in August (27%) at 313 hPa. During the years with
471 relative low ozone, Réunion is mainly influenced by tropical marine air and the
472 stratospheric influence is at a minimum. During the years with relative high ozone, the
473 stratospheric contribution reaches a maximum. The agreement between $StratO_3$, the
474 model ozone and observed ozone provides convincing evidence that the stratospheric
475 influence plays an important role in controlling the IAV of tropospheric ozone over
476 Réunion. Our examination of the horizontal wind pattern suggested that the IAV of large-
477 scale wind patterns could be an important factor in the changes from the stratospheric
478 contribution and also contribute to IAV of the ozone at 313 hPa. The simulated IAV of
479 tropospheric ozone between runs with interannually varying surface emissions and
480 constant emissions are almost identical (not shown), indicating that the IAV in emissions
481 does not contribute to the tropospheric ozone IAV over Réunion.

482 The GMI model captures the seasonality of observed trends, showing positive
483 trends during the July-September as well as during the December-January, notably in the

484 middle and upper troposphere. However, the model simulation underestimates the
485 observed magnitude of the maximum trend in July-September. For the Hindcast-VE
486 simulation, Réunion is located at the northernmost edge of the selected 2°x2.5° grid cell,
487 which centers at 22°S, 55°E. The mean value of ozone in this grid cell would be larger
488 than its northernmost edge value (21°S at Réunion) if the location of the large latitudinal
489 gradient in ozone moves to the South. The overestimate decreases when Réunion falls in
490 the high ozone region as the location with large latitudinal ozone gradient moves
491 northward. Therefore the changes in simulation errors due to coarse horizontal resolution
492 could buffer the actual changes. The magnitude of observed ozone trends from the
493 Réunion sondes are unlikely to be fully reproduced in the coarse-resolution 3-D model
494 (2°x2.5°). Increasing the spatial resolution of the simulation leads to somewhat better
495 agreement with the observed ozone mean mixing ratio, but the improvements varies year
496 by year. To fully capture the magnitude of observed trends, a simulation with even higher
497 resolution for both the horizontal and vertical grid, as well as an accurate representation
498 of the vertical transport processes and of the location of the sub-tropical jet may be
499 needed. Furthermore, our model analysis suggests that the frequency of sondes at
500 Reunion would have to be increased to give robust trends.

501 Many studies [e.g., *Pickering et al.*, 1990; *Lelieveld and Dentener*, 2000] have
502 shown that lightning NO_x is one of the important factors affecting tropospheric ozone in
503 the tropics, especially at the middle and upper troposphere. In our hindcast simulation,
504 lightning NOx are calculated online following the scheme described by Allen et al.
505 (2010), showing spatial variations, but with a constant global total value every year. A
506 recent study by Murray et al. [2013] compared the variance in the tropospheric ozone

column for 1998-2006 between a simulation using IAV in lightning from Lightning Imaging Sensor (LIS) and a base simulation with IAV only from GEOS convection. Their results show that the difference is exceedingly small at Réunion. We conclude that the lightning NO_x scheme in our hindcast simulation is not the reason for not fully capturing the observed ozone variability over Réunion.

The emission influence on the trends or IAV of tropospheric O3 reflects remote effects from emission sources through long-range transport. Increased emissions over the Eastern region contribute partially to the ozone increase in the upper troposphere in austral winter. Increasing emissions over southern Africa appears to affect only the lower troposphere and do not explain the observed trend maximum in the middle and upper troposphere during its austral winter season.

A recent model study by Li et al. [2010] based on simulations from a coupled chemistry-climate model (GEOSCCM) has identified a narrowing of the Hadley Cell's rising branch with enhanced descent extending into the tropics over the 21st century (2001-2099). Their simulations suggested that the expansion of the sinking branches of the Hadley Cell occurred on both the equatorward and poleward edges. The expansion of poleward edges is commonly referred as a widening of the tropical belt in various observational and modeling studies [e.g., *Hu and Fu*, 2007; *Seidel and Randel*, 2007]. The expansion of equatorward edges is associated with an equatorward movement and leads to the narrowing of the Hadley Cell's rising branch, which is likely to produce an increased stratospheric input over Réunion Island and result in increased tropospheric ozone near this region. Weekly ozonesonde measurements at this location will be promising for understanding the long-term variations in dynamical exchanges between

530 the tropics and mid-latitudes and between the troposphere and the stratosphere due to its
531 special location. It will also be valuable for evaluations of climate predictions from a
532 chemistry-climate model.
533
534 **Reference**

535 Baldy, S., G. Ancellet, M. Bessafi, A. Badr, and D. L. S. Luk (1996), Field observations
536 of the vertical distribution of tropospheric ozone at the island of Reunion (southern
537 tropics), *Journal of Geophysical Research-Atmospheres*, *101*(D19), 23835-23849,
538 doi:10.1029/95jd02929.
539 Baray, J. L., G. Ancellet, F. G. Taupin, M. Bessafi, S. Baldy, and P. Keckhut (1998),
540 Subtropical tropopause break as a possible stratospheric source of ozone in the
541 tropical troposphere, *Journal of Atmospheric and Solar-Terrestrial Physics*, *60*(1), 27-
542 36, doi:10.1016/s1364-6826(97)00116-8.
543 Baray, J. L., S. Baldy, R. D. Diab, and J. P. Cammas (2003), Dynamical study of a
544 tropical cut-off low over South Africa, and its impact on tropospheric ozone,
545 *Atmospheric Environment*, *37*(11), 1475-1488, doi:10.1016/s1352-2310(02000999-
546 8.
547 Baray, J. L., et al. (2006), An instrumented station for the survey of ozone and
548 climate change in the southern tropics, *Journal of Environmental Monitoring*, *8*(10),
549 1020-1028, doi:10.1039/b607762e.
550 Bell, M. L., F. Dominici, and J. M. Samet (2005), A meta-analysis of time-series studies
551 of ozone and mortality with comparison to the national morbidity, mortality, and air

552 pollution study, *Epidemiology*, *16*(4), 436-445,
553 doi:10.1097/01.ede.0000165817.40152.85.
554 Brewer, A. W. (1949), EVIDENCE FOR A WORLD CIRCULATION PROVIDED BY THE
555 MEASUREMENTS OF HELIUM AND WATER VAPOUR DISTRIBUTION IN THE
556 STRATOSPHERE, *Quarterly Journal of the Royal Meteorological Society*, *75*(326), 351-
557 363, doi:10.1002/qj.49707532603.
558 Chin, M., P. Ginoux, S. Kinne, O. Torres, B. N. Holben, B. N. Duncan, R. V. Martin, J. A.
559 Logan, A. Higurashi, and T. Nakajima (2002), Tropospheric aerosol optical thickness
560 from the GOCART model and comparisons with satellite and Sun photometer
561 measurements, *J ATMOS SCI*, *59*(3), 461-483.
562 Clain, G., J. L. Baray, R. Delmas, R. Diab, J. L. de Bellevue, P. Keckhut, F. Posny, J. M.
563 Metzger, and J. P. Cammas (2009), Tropospheric ozone climatology at two Southern
564 Hemisphere tropical/subtropical sites, (Reunion Island and Irene, South Africa)
565 from ozonesondes, LIDAR, and in situ aircraft measurements, *Atmospheric Chemistry*
566 *and Physics*, *9*(5), 1723-1734.
567 Cooper, O. R., et al. (2010), Increasing springtime ozone mixing ratios in the free
568 troposphere over western North America, *Nature*, *463*(7279), 344-348,
569 doi:10.1038/nature08708.
570 De Bellevue, J. L., J. L. Baray, S. Baldy, G. Ancellet, R. Diab, and F. Ravetta (2007),
571 Simulations of stratospheric to tropospheric transport during the tropical cyclone
572 Marlene event, *Atmospheric Environment*, *41*(31), 6510-6526,
573 doi:10.1016/j.atmosenv.2007.04.040.

574 Dobson, G. M. B. (1956), ORIGIN AND DISTRIBUTION OF THE POLYATOMIC
575 MOLECULES IN THE ATMOSPHERE, *Proceedings of the Royal Society of London Series*
576 *a-Mathematical and Physical Sciences*, *236*(1205), 187-193,
577 doi:10.1098/rspa.1956.0127.
578 Duncan, B. N., R. V. Martin, A. C. Staudt, R. Yevich, and J. A. Logan (2003), Interannual
579 and seasonal variability of biomass burning emissions constrained by satellite
580 observations, *Journal of Geophysical Research-Atmospheres*, *108*(D2),
581 doi:10.1029/2002jd002378.
582 Duncan, B. N., S. E. Strahan, Y. Yoshida, S. D. Steenrod, and N. Livesey (2007), Model
583 study of the cross-tropopause transport of biomass burning pollution, *ATMOS CHEM*
584 *PHYS*, *7*(14), 3713-3736.
585 Fiore, A. M., D. J. Jacob, B. D. Field, D. G. Streets, S. D. Fernandes, and C. Jang (2002),
586 Linking ozone pollution and climate change: The case for controlling methane,
587 *Geophysical Research Letters*, *29*(19), doi:10.1029/2002gl015601.
588 Forster, P. M., G. Bodeker, R. Schofield, S. Solomon, and D. Thompson (2007), Effects
589 of ozone cooling in the tropical lower stratosphere and upper troposphere,
590 *Geophysical Research Letters*, *34*(23), doi:10.1029/2007gl031994.
591 Fusco, A. C., and J. A. Logan (2003), Analysis of 1970-1995 trends in tropospheric
592 ozone at Northern Hemisphere midlatitudes with the GEOS-CHEM model, *Journal of*
593 *Geophysical Research-Atmospheres*, *108*(D15), doi:10.1029/2002jd002742.
594 Garstang, M., P. D. Tyson, R. Swap, M. Edwards, P. Kallberg, and J. A. Lindesay (1996),
595 Horizontal and vertical transport of air over southern Africa, *Journal of Geophysical*
596 *Research-Atmospheres*, *101*(D19), 23721-23736, doi:10.1029/95jd00844.

597 Guenther, A., T. Karl, P. Harley, C. Wiedinmyer, P. I. Palmer, and C. Geron (2006),
598 Estimates of global terrestrial isoprene emissions using MEGAN (Model of
599 Emissions of Gases and Aerosols from Nature), *ATMOS CHEM PHYS*, *6*, 3181-3210.
600 Hastenrath, S., and M. C. Wu (1982), OSCILLATIONS OF UPPER-AIR CIRCULATION
601 AND ANOMALIES IN THE SURFACE CLIMATE OF THE TROPICS, *Archives for*
602 *Meteorology Geophysics and Bioclimatology Series B-Theoretical and Applied*
603 *Climatology*, *31*(1-2), 1-37, doi:10.1007/bf02311340.
604 Hess, P. G., D. Kinnison, and Q. Tang (2015), Ensemble simulations of the role of the
605 stratosphere in the attribution of tropospheric ozone variability, *Atmos. Chem. Phys.*,
606 *15*, 2341-2365, doi:2310.5194/acp-2315-2341-2015, 2015.
607 Hess, P. G., and R. Zbinden (2013), Stratospheric impact on tropospheric ozone
608 variability and trends: 1990-2009, *Atmospheric Chemistry and Physics*, *13*(2), 649-
609 674, doi:10.5194/acp-13-649-2013.
610 Holton, J. R., P. H. Haynes, M. E. McIntyre, A. R. Douglass, R. B. Rood, and L. Pfister
611 (1995), STRATOSPHERE-TROPOSPHERE EXCHANGE, *Reviews of Geophysics*, *33*(4),
612 403-439, doi:10.1029/95rg02097.
613 Hoskins, B. J., and M. J. Rodwell (1995), A MODEL OF THE ASIAN SUMMER
614 MONSOON .1. THE GLOBAL-SCALE, *Journal of the Atmospheric Sciences*, *52*(9), 1329-
615 1340, doi:10.1175/1520-0469(1995)052<1329:amotas>2.0.co;2.
616 Hu, Y., and Q. Fu (2007), Observed poleward expansion of the Hadley circulation
617 since 1979, *Atmospheric Chemistry and Physics*, *7*(19), 5229-5236.
618 Karlsdottir, S., I. S. A. Isaksen, G. Myhre, and T. K. Berntsen (2000), Trend analysis of
619 O-3 and CO in the period 1980-1996: A three-dimensional model study, *Journal of*

620 *Geophysical Research-Atmospheres*, *105*(D23), 28907-28933,
621 doi:10.1029/2000jd900374.
622 Lacis, A. A., D. J. Wuebbles, and J. A. Logan (1990), RADIATIVE FORCING OF
623 CLIMATE BY CHANGES IN THE VERTICAL-DISTRIBUTION OF OZONE, *Journal of*
624 *Geophysical Research-Atmospheres*, *95*(D7), 9971-9981,
625 doi:10.1029/JD095iD07p09971.
626 Lelieveld, J., and F. J. Dentener (2000), What controls tropospheric ozone?, *Journal of*
627 *Geophysical Research-Atmospheres*, *105*(D3), 3531-3551,
628 doi:10.1029/1999jd901011.
629 Lelieveld, J., J. van Aardenne, H. Fischer, M. de Reus, J. Williams, and P. Winkler
630 (2004), Increasing ozone over the Atlantic Ocean, *Science*, *304*(5676), 1483-1487,
631 doi:10.1126/science.1096777.
632 Li, F., R. S. Stolarski, S. Pawson, P. A. Newman, and D. Waugh (2010), Narrowing of
633 the upwelling branch of the Brewer-Dobson circulation and Hadley cell in
634 chemistry-climate model simulations of the 21st century, *Geophysical Research*
635 *Letters*, *37*, doi:10.1029/2010gl043718.
636 Lin, M., A. M. Fiore, O. R. Cooper, L. W. Horowitz, A. O. Langford, H. Levy II, B. J.
637 Johnson, V. Vaishali Naik, S. J. Oltmans, and C. J. Senff (2012), Springtime high
638 surface ozone events over the western United States: Quantifying the role of
639 stratospheric intrusions, *Submitted to JGR-Atmosphere, CalNex Special Section*.
640 Lin, M., A. M. Fiore, L. W. Horowitz, A. O. Langford, S. J. Oltmans, D. Tarasick, and H. E.
641 Rieder (2015), Climate variability modulates western US ozone air quality in spring

642 via deep stratospheric intrusions, *Nature Communications*, *6*,
643 doi:10.1038/ncomms8105.
644 Lin, M., L. W. Horowitz, S. J. Oltmans, A. M. Fiore, and S. Fan (2014), Tropospheric
645 ozone trends at Mauna Loa Observatory tied to decadal climate variability, *Nature*
646 *Geoscience*, *7*(2), 136-143, doi:10.1038/ngeo2066.
647 Logan, J. A. (1999), An analysis of ozonesonde data for the troposphere:
648 Recommendations for testing 3-D models and development of a gridded climatology
649 for tropospheric ozone, *Journal of Geophysical Research-Atmospheres*, *104*(D13),
650 16115-16149, doi:10.1029/1998jd100096.
651 Logan, J. A., and V. Kirchhoff (1986), SEASONAL-VARIATIONS OF TROPOSPHERIC
652 OZONE AT NATAL, BRAZIL, *Journal of Geophysical Research-Atmospheres*, *91*(D7),
653 7875-7881, doi:10.1029/JD091iD07p07875.
654 Logan, J. A., I. Megretskaia, R. Nassar, L. T. Murray, L. Zhang, K. W. Bowman, H. M.
655 Worden, and M. Luo (2008), Effects of the 2006 El Nino on tropospheric
656 composition as revealed by data from the Tropospheric Emission Spectrometer
657 (TES), *Geophysical Research Letters*, *35*(3), doi:10.1029/2007gl031698.
658 Logan, J. A., M. J. Prather, S. C. Wofsy, and M. B. McElroy (1981), TROPOSPHERIC
659 CHEMISTRY - A GLOBAL PERSPECTIVE, *Journal of Geophysical Research-Oceans and*
660 *Atmospheres*, *86*(NC8), 7210-7254, doi:10.1029/JC086iC08p07210.
661 Logan, J. A., et al. (2012), Changes in ozone over Europe: Analysis of ozone
662 measurements from sondes, regular aircraft (MOZAIC) and alpine surface sites,
663 *Journal of Geophysical Research-Atmospheres*, *117*, doi:10.1029/2011jd016952.

McLinden, C. A., S. C. Olsen, B. Hannegan, O. Wild, M. J. Prather, and J. Sundet (2000), Stratospheric ozone in 3-D models: A simple chemistry and the cross-tropopause flux, *Journal of Geophysical Research-Atmospheres*, *105*(D11), 14653-14665, doi:10.1029/2000jd900124.

Moorthi, S., and M. J. Suarez (1992), RELAXED ARAKAWA-SCHUBERT - A PARAMETERIZATION OF MOIST CONVECTION FOR GENERAL-CIRCULATION MODELS, *Monthly Weather Review*, *120*(6), 978-1002, doi:10.1175/1520-0493(1992)120<0978:rasapo>2.0.co;2.

Murray, L. T., J. A. Logan, and D. J. Jacob (2013), Interannual variability in tropical tropospheric ozone and OH: The role of lightning, *Journal of Geophysical Research-Atmospheres*, *118*(19), 11468-11480, doi:10.1002/jgrd.50857.

Olivier, J. G. J., J. A. Van Aardenne, F. J. Dentener, V. Pagliari, L. N. Ganzeveld, and J. A. H. W. Peters (2005), Recent trends in global greenhouse gas emissions: regional trends and spatial distribution of key sources, in *Non-CO2 Greenhouse Gases (NCGG-4), coordinator: van Amstel, A., Millpress, Rotterdam, ISBN 905966 043 9, 325–330,*, edited.

Pickering, K. E., A. M. Thompson, R. R. Dickerson, W. T. Luke, D. P. McNamara, J. P. Greenberg, and P. R. Zimmerman (1990), MODEL-CALCULATIONS OF TROPOSPHERIC OZONE PRODUCTION POTENTIAL FOLLOWING OBSERVED CONVECTIVE EVENTS, *Journal of Geophysical Research-Atmospheres*, *95*(D9), 14049-14062, doi:10.1029/JD095iD09p14049.

Piketh, S. J., R. J. Swap, W. Maenhaut, H. J. Annegam, and P. Formenti (2002), Chemical evidence of long-range atmospheric transport over southern Africa,

687 *Journal of Geophysical Research-Atmospheres*, *107*(D24),
688 doi:10.1029/2002jd002056.
689 Postel, G. A., and M. H. Hitchman (1999), A climatology of Rossby wave breaking
690 along the subtropical tropopause, *Journal of the Atmospheric Sciences*, *56*(3), 359-
691 373, doi:10.1175/1520-0469(1999)056<0359:acorwb>2.0.co;2.
692 Pozzoli, L., G. Janssens-Maenhout, T. Diehl, I. Bey, M. G. Schultz, J. Feichter, E. Vignati,
693 and F. Dentener (2011), Re-analysis of tropospheric sulfate aerosol and ozone for
694 the period 1980-2005 using the aerosol-chemistry-climate model ECHAM5-
695 HAMMOZ, *Atmospheric Chemistry and Physics*, *11*(18), 9563-9594, doi:10.5194/acp-
696 11-9563-2011.
697 Prather, M. J., X. Zhu, Q. Tang, J. N. Hsu, and J. L. Neu (2011), An atmospheric chemist
698 in search of the tropopause, *J GEOPHYS RES-ATMOS*, *116*, D04306,
699 doi:10.1029/2010jd014939.
700 Randriambelo, T., J. L. Baray, and S. Baldy (2000), Effect of biomass burning,
701 convective venting, and transport on tropospheric ozone over the Indian Ocean:
702 Reunion Island field observations, *Journal of Geophysical Research-Atmospheres*,
703 *105*(D9), 11813-11832, doi:10.1029/1999jd901097.
704 Randriambelo, T., J. L. Baray, S. Baldy, A. M. Thompson, S. Oltmans, and P. Keckhut
705 (2003), Investigation of the short-time variability of tropical tropospheric ozone,
706 *Annales Geophysicae*, *21*(10), 2095-2106.
707 Rienecker, M. M., et al. (2011), MERRA: NASA's Modern-Era Retrospective Analysis
708 for Research and Applications, *Journal of Climate*, *24*(14), 3624-3648,
709 doi:10.1175/jcli-d-11-00015.1.

710 Rodwell, M. J., and B. J. Hoskins (2001), Subtropical anticyclones and summer
711 monsoons, *Journal of Climate*, *14*(15), 3192-3211, doi:10.1175/1520-
712 0442(2001)014<3192:saasm>2.0.co;2.
713 Saunois, M., L. Emmons, J. F. Lamarque, S. Tilmes, C. Wespes, V. Thouret, and M.
714 Schultz (2012), Impact of sampling frequency in the analysis of tropospheric ozone
715 observations, *Atmospheric Chemistry and Physics*, *12*(15), 6757-6773,
716 doi:10.5194/acp-12-6757-2012.
717 Sauvage, B., R. V. Martin, A. van Donkelaar, and J. R. Ziemke (2007), Quantification of
718 the factors controlling tropical tropospheric ozone and the South Atlantic maximum,
719 *Journal of Geophysical Research-Atmospheres*, *112*(D11),
720 doi:10.1029/2006jd008008.
721 Sauvage, B., V. Thouret, A. M. Thompson, J. C. Witte, J. P. Cammas, P. Nedelec, and G.
722 Athier (2006), Enhanced view of the "tropical Atlantic ozone paradox'' and "zonal
723 wave one'' from the in situ MOZAIC and SHADOZ data, *Journal of Geophysical*
724 *Research-Atmospheres*, *111*(D1), doi:10.1029/2005jd006241.
725 Seidel, D. J., and W. J. Randel (2007), Recent widening of the tropical belt: Evidence
726 from tropopause observations, *Journal of Geophysical Research-Atmospheres*,
727 *112*(D20), doi:10.1029/2007jd008861.
728 Senten, C., et al. (2008), Technical note: New ground-based FTIR measurements at
729 Ile de La Reunion: observations, error analysis, and comparisons with independent
730 data, *Atmospheric Chemistry and Physics*, *8*(13), 3483-3508.

731 Silva, R. A., et al. (2013), Global premature mortality due to anthropogenic outdoor
732 air pollution and the contribution of past climate change, *Environmental Research*
733 *Letters*, *8*(3), doi:10.1088/1748-9326/8/3/034005.
734 Sitch, S., P. M. Cox, W. J. Collins, and C. Huntingford (2007), Indirect radiative forcing
735 of climate change through ozone effects on the land-carbon sink, *Nature*, *448*(7155),
736 791-U794, doi:10.1038/nature06059.
737 Skerlak, B., M. Sprenger, and H. Wernli (2014), A global climatology of stratosphere-
738 troposphere exchange using the ERA-Interim data set from 1979 to 2011,
739 *Atmospheric Chemistry and Physics*, *14*(2), 913-937, doi:10.5194/acp-14-913-2014.
740 Stevenson, D. S., et al. (2013), Tropospheric ozone changes, radiative forcing and
741 attribution to emissions in the Atmospheric Chemistry and Climate Model
742 Intercomparison Project (ACCMIP), *Atmospheric Chemistry and Physics*, *13*(6), 3063-
743 3085, doi:10.5194/acp-13-3063-2013.
744 Stolarski, R. S., A. R. Douglass, S. Steenrod, and S. Pawson (2006), Trends in
745 stratospheric ozone: Lessons learned from a 3D chemical transport model, *J ATMOS*
746 *SCI*, *63*(3), 1028-1041.
747 Strahan, S. E., B. N. Duncan, and P. Hoor (2007), Observationally derived transport
748 diagnostics for the lowermost stratosphere and their application to the GMI
749 chemistry and transport model, *ATMOS CHEM PHYS*, *7*(9), 2435-2445.
750 Sudo, K., and H. Akimoto (2007), Global source attribution of tropospheric ozone:
751 Long-range transport from various source regions, *Journal of Geophysical Research-*
752 *Atmospheres*, *112*(D12), doi:10.1029/2006jd007992.

753 Taupin, F. G., M. Bessafi, S. Baldy, and P. J. Bremaud (1999), Tropospheric ozone
754 above the southwestern Indian Ocean is strongly linked to dynamical conditions
755 prevailing in the tropics, *Journal of Geophysical Research-Atmospheres*, *104*(D7),
756 8057-8066, doi:10.1029/98jd02456.
757 Thompson, A. M., N. V. Balashov, J. C. Witte, J. G. R. Coetzee, V. Thouret, and F. Posny
758 (2014), Tropospheric ozone increases over the southern Africa region: bellwether
759 for rapid growth in Southern Hemisphere pollution?, *Atmospheric Chemistry and*
760 *Physics*, *14*(18), 9855-9869, doi:10.5194/acp-14-9855-2014.
761 Thompson, A. M., et al. (2012), Southern Hemisphere Additional Ozonesondes
762 (SHADOZ) ozone climatology (2005-2009): Tropospheric and tropical tropopause
763 layer (TTL) profiles with comparisons to OMI-based ozone products, *Journal of*
764 *Geophysical Research-Atmospheres*, *117*, doi:10.1029/2011jd016911.
765 Thompson, A. M., K. E. Pickering, D. P. McNamara, M. R. Schoeberl, R. D. Hudson, J. H.
766 Kim, E. V. Browell, V. Kirchhoff, and D. Nganga (1996), Where did tropospheric
767 ozone over southern Africa and the tropical Atlantic come from in October 1992?
768 Insights from TOMS, GTE TRACE A, and SAFARI 1992, *Journal of Geophysical*
769 *Research-Atmospheres*, *101*(D19), 24251-24278, doi:10.1029/96jd01463.
770 Thompson, A. M., et al. (2003), Southern Hemisphere Additional Ozonesondes
771 (SHADOZ) 1998-2000 tropical ozone climatology - 1. Comparison with Total Ozone
772 Mapping Spectrometer (TOMS) and ground-based measurements, *Journal of*
773 *Geophysical Research-Atmospheres*, *108*(D2), doi:10.1029/2001jd000967.
774 Thompson, A. M., J. C. Witte, H. G. J. Smit, S. J. Oltmans, B. J. Johnson, V. W. J. H.
775 Kirchhoff, and F. J. Schmidlin (2007), Southern Hemisphere Additional Ozonesondes

776 (SHADOZ) 1998-2004 tropical ozone climatology: 3. Instrumentation, station-to-
777 station variability, and evaluation with simulated flight profiles, *Journal of*
778 *Geophysical Research-Atmospheres*, *112*(D3), doi:10.1029/2005jd007042.
779 van der Werf, G. R., J. T. Randerson, L. Giglio, G. L. Collatz, M. Mu, P. S. Kasibhatla, D.
780 C. Morton, R. S. DeFries, Y. Jin, and v. L. T.T. (2010), Global fire emissions and the
781 contribution of deforestation, savanna, forest, agricultural, and peat fires (1997–
782 2009), *ATMOS CHEM PHYS*, *10*, 16153-16230.
783 Wargan, K., S. Pawson, M. A. Olsen, J. C. Witte, A. R. Douglass, J. R. Ziemke, S. E.
784 Strahan, and J. E. Nielsen (2015), The global structure of upper troposphere-lower
785 stratosphere ozone in GEOS-5: A multiyear assimilation of EOS Aura data, *Journal of*
786 *Geophysical Research-Atmospheres*, *120*(5), 2013-2036, doi:10.1002/2014jd022493.
787 Waugh, D. W., and L. M. Polvani (2000), Climatology of intrusions into the tropical
788 upper troposphere, *Geophysical Research Letters*, *27*(23), 3857-3860,
789 doi:10.1029/2000gl012250.
790 Ziemke, J. R., S. Chandra, and P. K. Bhartia (2001), "Cloud slicing": A new technique
791 to derive upper tropospheric ozone from satellite measurements, *Journal of*
792 *Geophysical Research-Atmospheres*, *106*(D9), 9853-9867,
793 doi:10.1029/2000jd900768.
794 Ziemke, J. R., S. Chandra, R. D. McPeters, and P. A. Newman (1997), Dynamical
795 proxies of column ozone with applications to global trend models, *Journal of*
796 *Geophysical Research-Atmospheres*, *102*(D5), 6117-6129, doi:10.1029/96jd03783.
797 Ziemke, J. R., et al. (2014), Assessment and applications of NASA ozone data
798 products derived from Aura OMI/MLS satellite measurements in context of the GMI

799 chemical transport model, *Journal of Geophysical Research-Atmospheres*, *119*(9),
800 5671-5699, doi:10.1002/2013jd020914.
801

802 **Figures:**

803 **Figure 1:** Temporal evolution of ozone profiles from Réunion ozonesonde in July and
804 August from 1992 to 2014. High-resolution Réunion sonde profiles are integrated to
805 MERRA reduced vertical grid (47 fixed pressure levels).

806

807 **Figure 2:** comparison of simulated monthly mean ozone mixing ratio averaged from the
808 GMI-CTM Hindcast-VE-HR run (1x1.25, with varying emissions) co-sampled with the
809 available sonde observations (red), and the mean determined from daily ozone fields
810 archived from the model (green) for July and August from 1992 to 2014 at 226 hPa, 313
811 hPa, and 510 hPa. Numbers in each panel represent the calculated linear trends at the
812 90% confidence level with unit ppb/decade. They follow the same color scheme as the
813 lines.

814 **Figure 3:** Comparison of GMI-CTM Hindcast-VE (2x2.5, red lines), Hindcast-VE-HR
815 (1x1.25, blue lines) and observed (black lines) monthly mean averaged over 1992 to 2002
816 (left panels) and 2003 to 2014 (right panels) at 226 hPa, 313 hPa, 510 hPa, and 694 hPa.
817 Vertical bars indicate ±2 standard error of the monthly mean values. The model results
818 are sampled on the date of sonde measurements. High-resolution Réunion sonde profiles
819 are integrated to MERRA reduced vertical grid (47 fixed pressure levels).

820

821 **Figure 4:** Seasonal maps of tropospheric partial column ozone (in Dobson Unites,
822 integrated from 500 hPa to the tropopause) for December-February (DJF), March-May
823 (MAM), June-August (JJA), and September-November (SON) season averaged from
824 2005 to 2012 for GMAO assimilated ozone (left) and GMI-CTM Hindcast-VE ozone

825 (middle) and their absolute difference (right). The GMAO assimilated ozone has been
826 adjusted by adding 2.5 DU based on Wargan et al. [2015].
827
828 **Figure 5:** Time series of observed (black) and GMI-CTM Hindcast-VE simulated (red)
829 ozone mixing ratios, and the $StratO_3/O_3$ ratio (blue) at 313 hPa in July (left panels) and
830 August (right panels) from 1992 to 2014. The model results are sampled on the date of
831 sonde measurements.
832
833 **Figure 6:** Time series of observed (black) and GMI-CTM Hindcast-VE simulated (red)
834 ozone mixing ratios, and the $StratO_3/O_3$ ratio (blue) at 313 hPa in December from 1992 to
835 2014. The model results are sampled on the date of sonde measurements.
836
837 **Figure 7:** The monthly mean GMI-CTM Hindacast-VE simulated ozone mixing ratio at
838 313 hPa in July a) 1997 and b) 2006. And the simulated monthly mean $StratO_3/O_3$ ratio in
839 July c) 1997 and d) 2006. The black star denote the Réunion Island.
840
841 **Figure 8:** The profile of the monthly mean ozone in July (left) 1997 and (right) 2006
842 from Réunion sonde observations (black), GMI-CTM Hindcast-VE (red) and GMI-CTM
843 Hindcast-VE-HR simulations (blue). The model results are sampled on the date of sonde
844 measurements.
845

Figure 9: Monthly mean ozone mixing ratio (ppb) overlaid with horizontal winds derived from MERRA metfields in July 1997 (top) and 2006 (bottom) at 313 hPa for the GMI Hindcast-VE simulation. The black star denotes the Réunion.

Figure 10: Trend (ppb/decade) computed from a linear regression model for ozone profile data from a) Réunion sonde, b) Hindcast-VE from 1992 to 2014. The model results are sampled on the date of sonde measurements. Black line contour denotes statistical significance at 90% CI. "# of mons" at the bottom of Fig. 10a shows the number of data points in the trend calculation for that month in our regression model.

Figure 11: Temporal variation of emission of total NO (solid line), NO from fossil fuel (dash line) and NO from biomass burning (dash dot line) in our model in July-September from 1992 to 2011 over southern Africa and East regions. Numbers in each panel represent the calculated linear trends at the 90% confidence level with unit kt/mon/year.

Figure 12: Trend (ppb/decade) computed from a linear regression model for monthly mean ozone profiles, calculated from daily profiles sampled at sonde time, from a) Hindcast-CE, b) Hindcast-VE from 1992-2011. Right panel is the difference of the trends between these two runs in unit ppb/decade.

Acknowledgement

All model output used for this article can be obtained by contacting J. Liu (email:Junhua.liu@nasa.gov). I gratefully acknowledge the financial support by NASA's Atmospheric Chemistry Modeling and Analysis Program (ACMAP) (grants NNH12ZDA001N). Work was performed under contract with NASA at Goddard. The sonde program at Réunion was initiated in 1991/1992 with the support of the CNRS and the University of La Réunion; after 1997, additional funding came SHADOZ through the Upper Atmosphere Research Program of NASA (thanks to M. J. Kurylo and K. W. Jucks) with contributions from NOAA/GMD and NASA's Aura Validation. Thanks to J. L. Baray (the LaMP/OPGC, FRANCE) for sonde data from September 1992 to December 1997. Sonde data after 1998 can be obtained from SHADOZ website (http://croc.gsfc.nasa.gov/shadoz/). Thanks to J. M. Metzger (University of La Réunion) for on-going technical support of the sounding program. I would like to thank S. Pawson and K. Wargan for their helpful discussion on GMAO assimilated ozone products. I benefited from useful discussions with J. Ziemke.

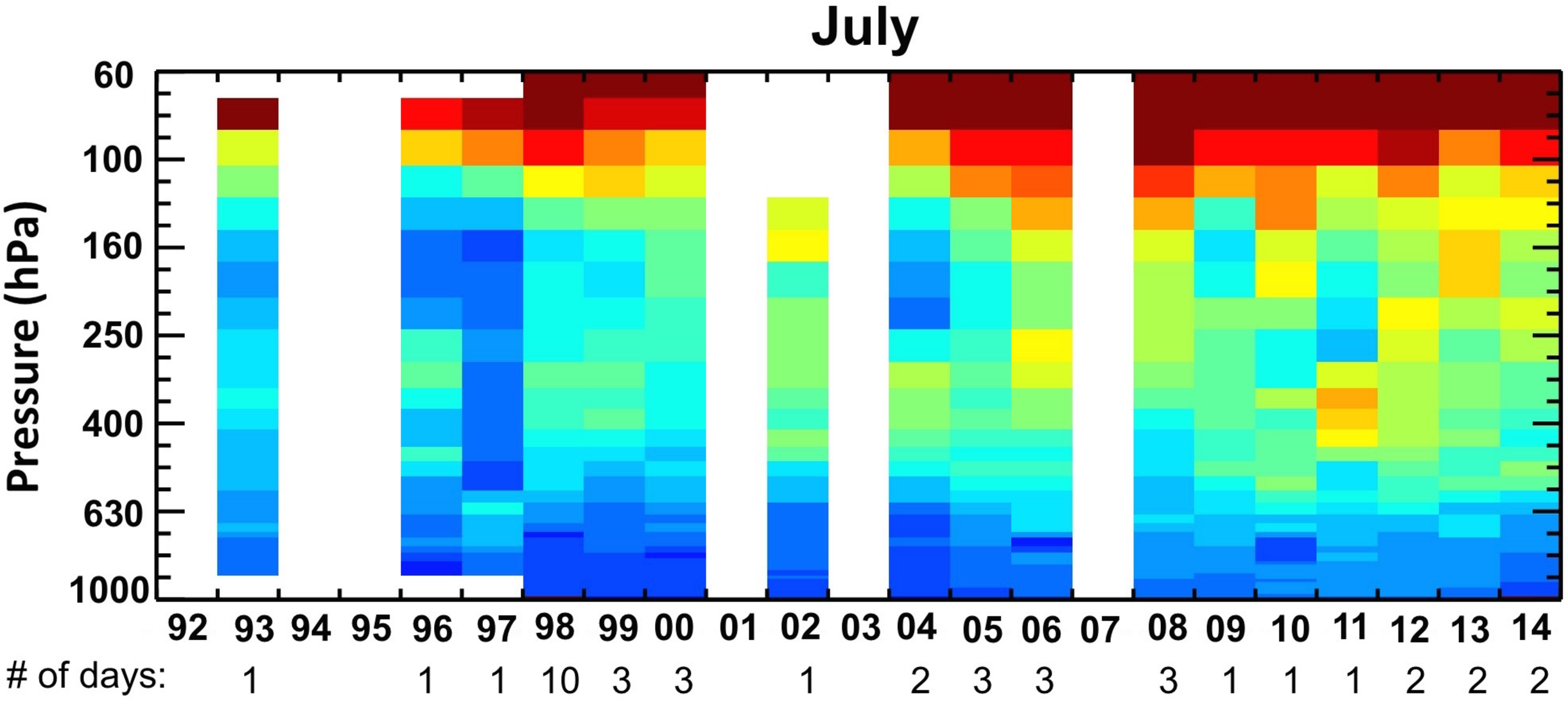
July
Pressure (hPa)
60
100
160
250
400
630
1000
92 93 94 95 96 97 98 99 00 01 02 03 04 05 06 07 08 09 10 11 12 13 14
# of days:
1 1 1 10 3 3 1 2 3 3 3 1 1 1 2 2 2

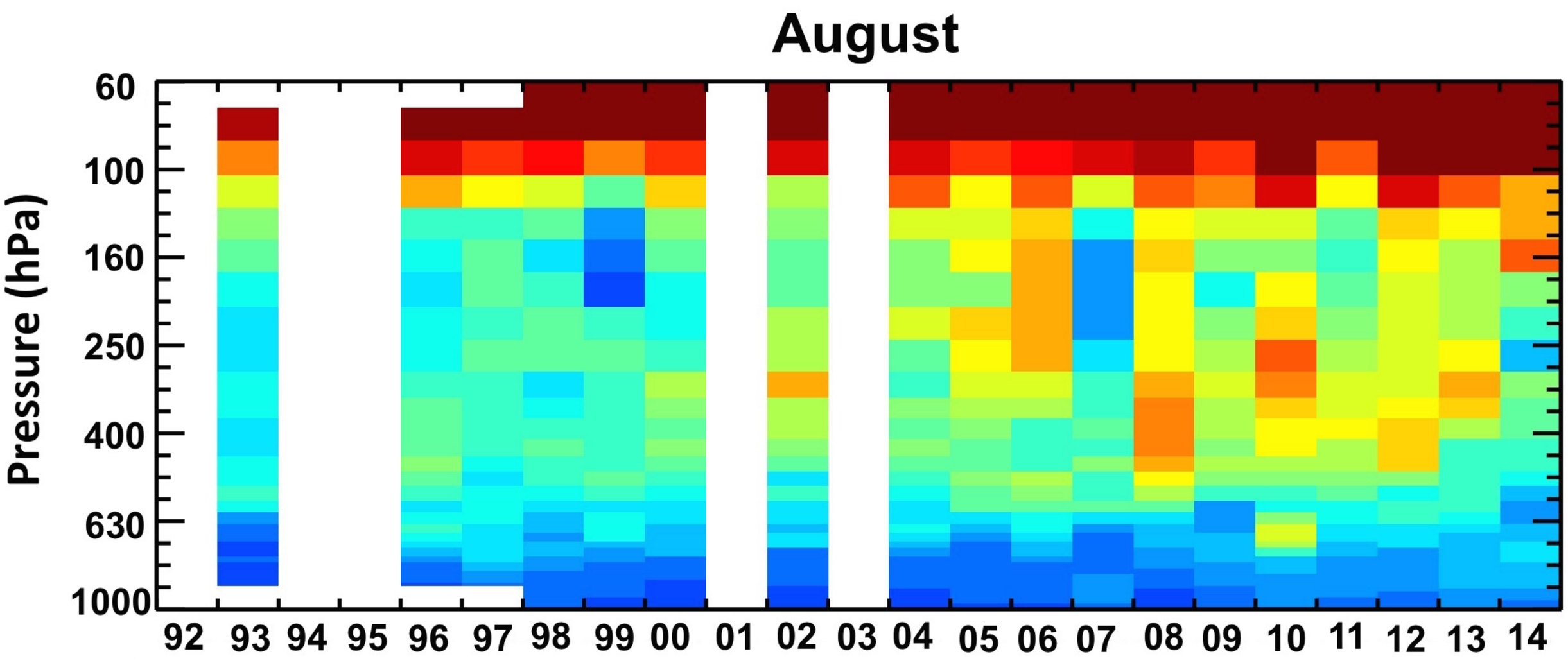
August
Pressure (hPa)
60
100
160
250
400
630
1000
92 93 94 95 96 97 98 99 00 01 02 03 04 05 06 07 08 09 10 11 12 13 14
# of days:
2 2 1 1 4 1 2 2 2 1 2 1 1 1 3 1 2 1
Year


ppb
<
0
45
90
135

HFF2HR-sampled
HFF2HR-daily

Jul at 226 hPa

7.40+- 8.64
5.95+- 3.77

Aug at 226 hPa

12.56+- 10.47
4.79+- 5.47

Jul at 313 hPa

4.64+- 8.03
3.48+- 2.85

Aug at 313 hPa

9.94+- 9.45
3.98+- 3.8

Jul at 510 hPa

3.84+- 4.49
0.62+- 2.06

Aug at 510 hPa

0.17+- 4.49
2.64+- 1.58

O3 (ppb)

120
100
80
60
40
20

92
97
02
07
12

Year

1992-2002

2003-2014

226 hPa

313 hPa

510 hPa

694 hPa

O3 (ppb)

120
100
80
60
40
20
0

Jan Mar May Jul Sep Nov

Month

O3-sondes
O3-Hindcast-VE
O3-Hindcast-VE-HR

Averaged over 2005-2012

GMAO TOC + 2.5 DU

GMI TOC

GMI - GMAO

DJF

MAM

JJA

SON

0°
10°S
20°S
30°S
40°S
50°S

180° 120°W 60°W 0° 60°E 120°E 180°

0 7 15 22 30 DU

-10 -5 0 5 10 DU

July

O3 (ppb)

O3-Sondes

O3-Hindcast-VE

r(sonde-model) = 0.78

StratO3/TotalO3 %

StratO3/O3

r(model-StratO3/O3) = 0.66

Year

August

O3 (ppb)

O3-Sondes

O3-Hindcast-VE

r(sonde-model) = 0.52

StratO3/TotalO3 %

StratO3/O3

r(model-StratO3/O3) = 0.42

Year

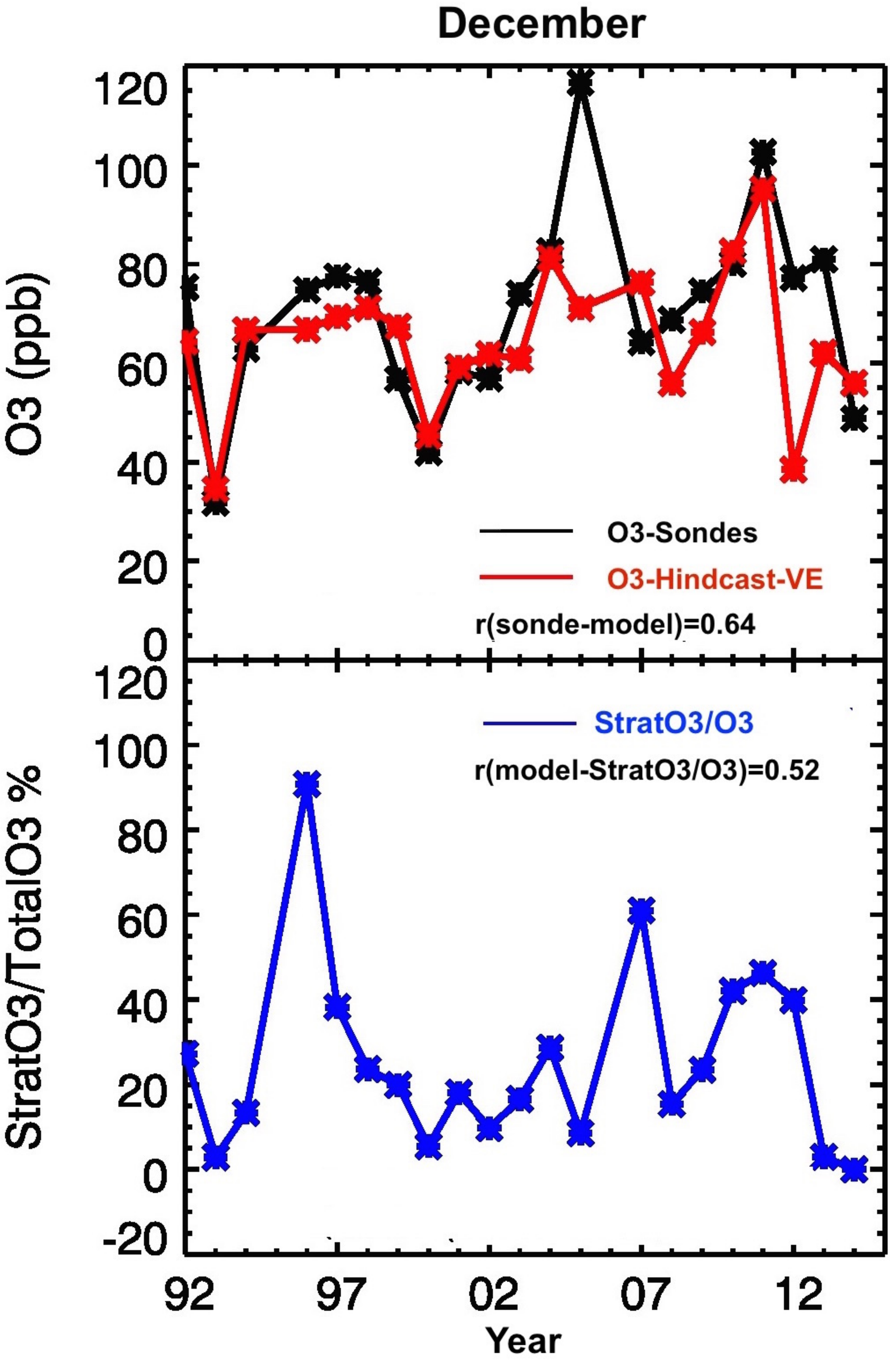
December
O3 (ppb)
120
100
80
60
40
20
0
O3-Sondes
O3-Hindcast-VE
r(sonde-model)=0.64
StratO3/TotalO3 %
120
100
80
60
40
20
0
-20
StratO3/O3
r(model-StratO3/O3)=0.52
92
97
02
07
12
Year

a) O3, July 1997 at 313 hPa

b) O3, July 2006 at 313 hPa

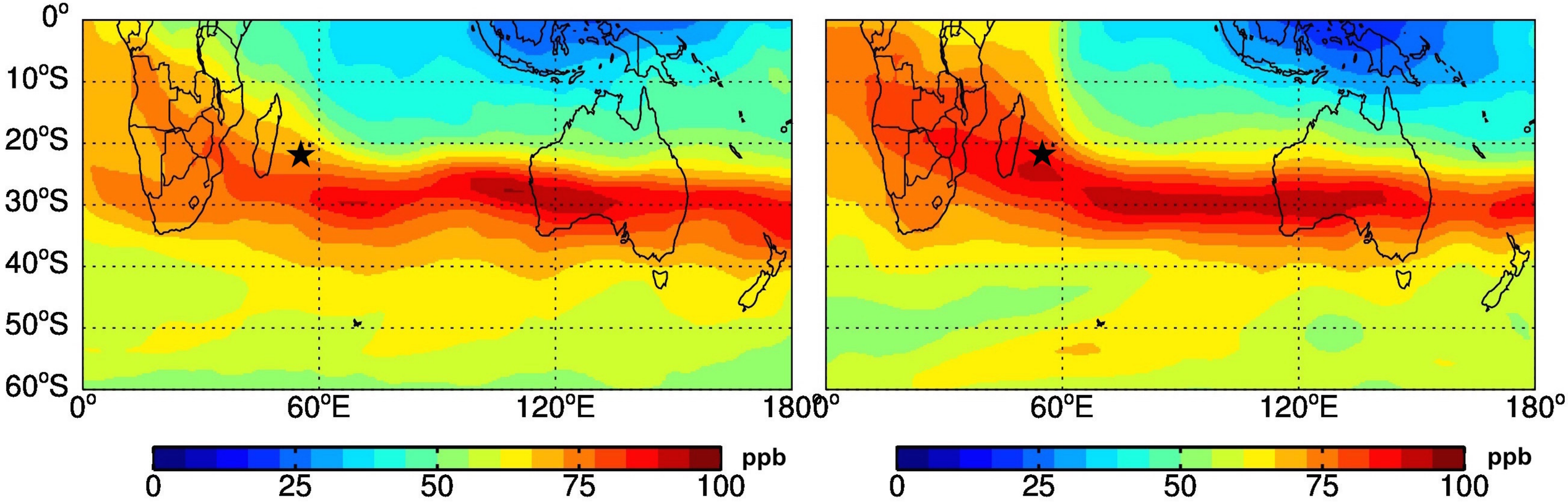

c) StratO3/O3, July 1997 at 313 hPa

d) StratO3/O3, July 2006 at 313 hPa

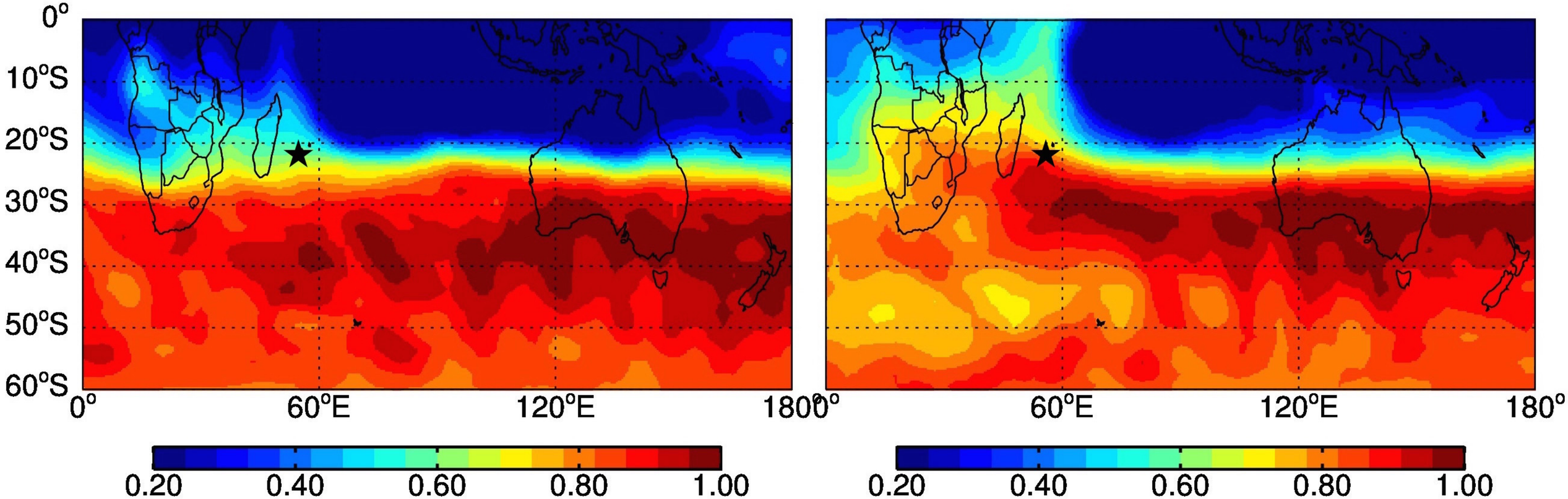

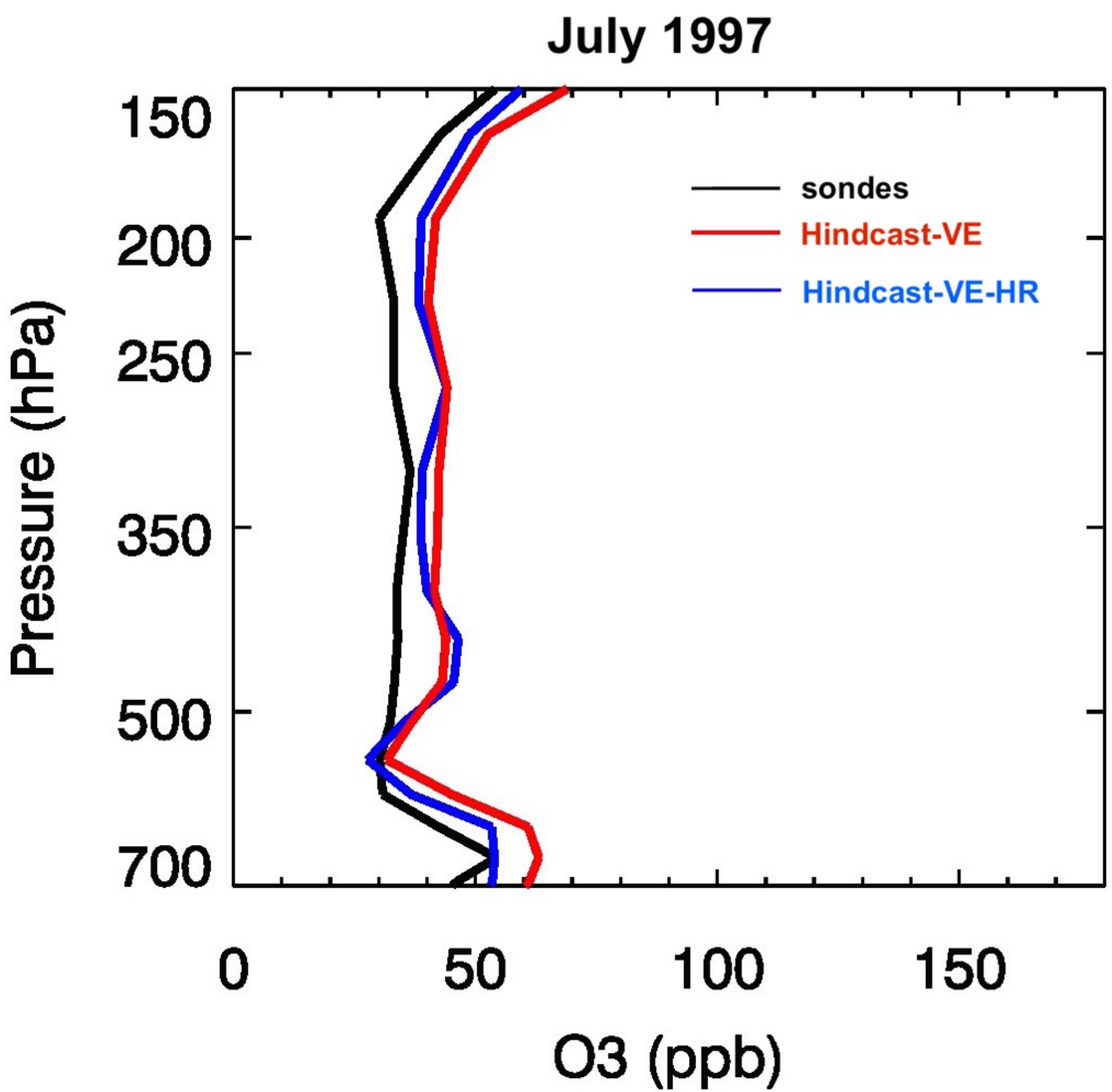
July 1997
150
200
250
350
500
700
Pressure (hPa)
sondes
Hindcast-VE
Hindcast-VE-HR
0
50
100
150
O3 (ppb)

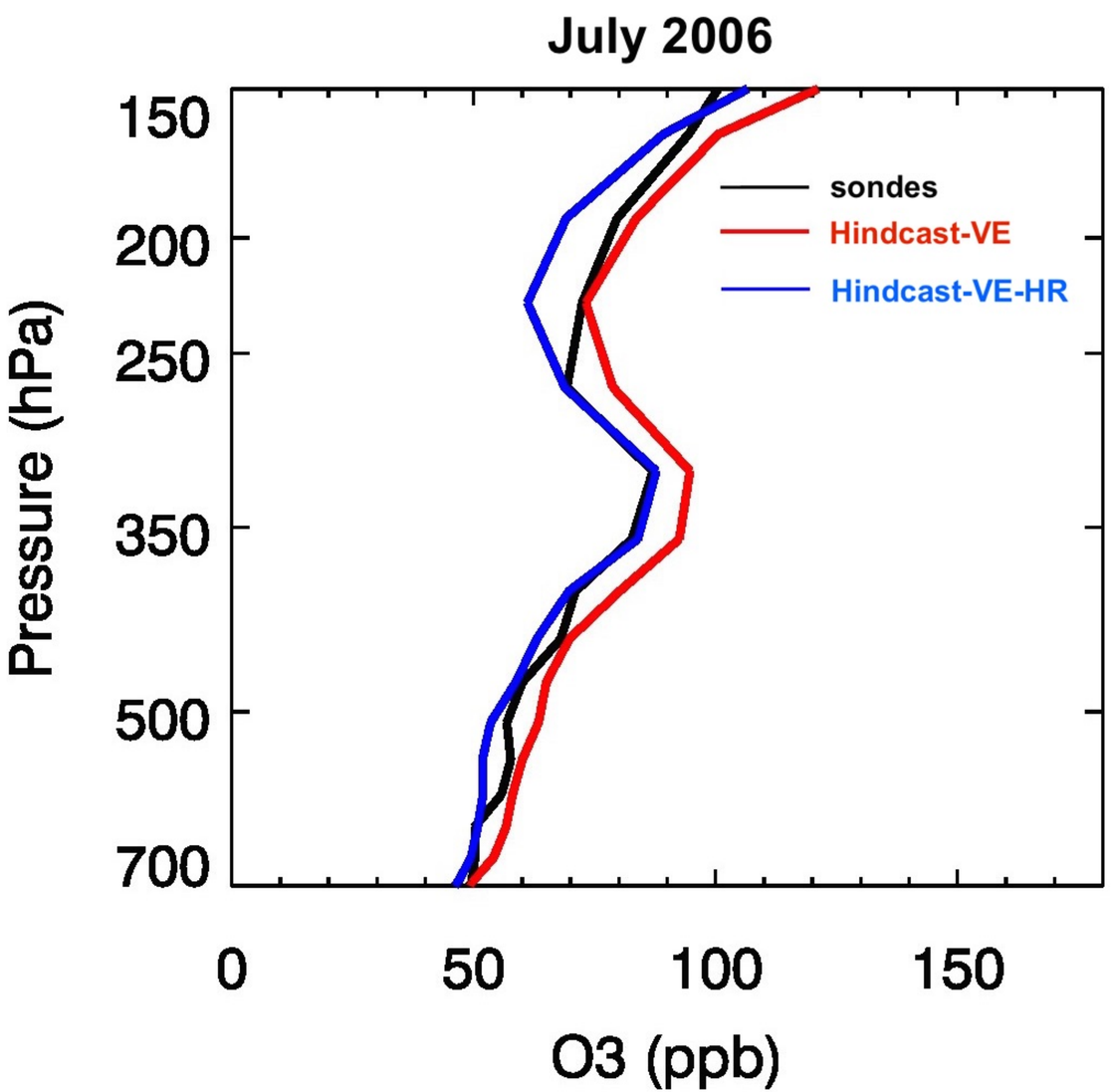
July 2006
150
200
250
350
500
700
Pressure (hPa)
sondes
Hindcast-VE
Hindcast-VE-HR
0
50
100
150
O3 (ppb)

July 1997, 313 hPa

0°
10°S
20°S
30°S
40°S
50°S
60°S
0°
60°E
120°E
180°

July 2006, 313 hPa

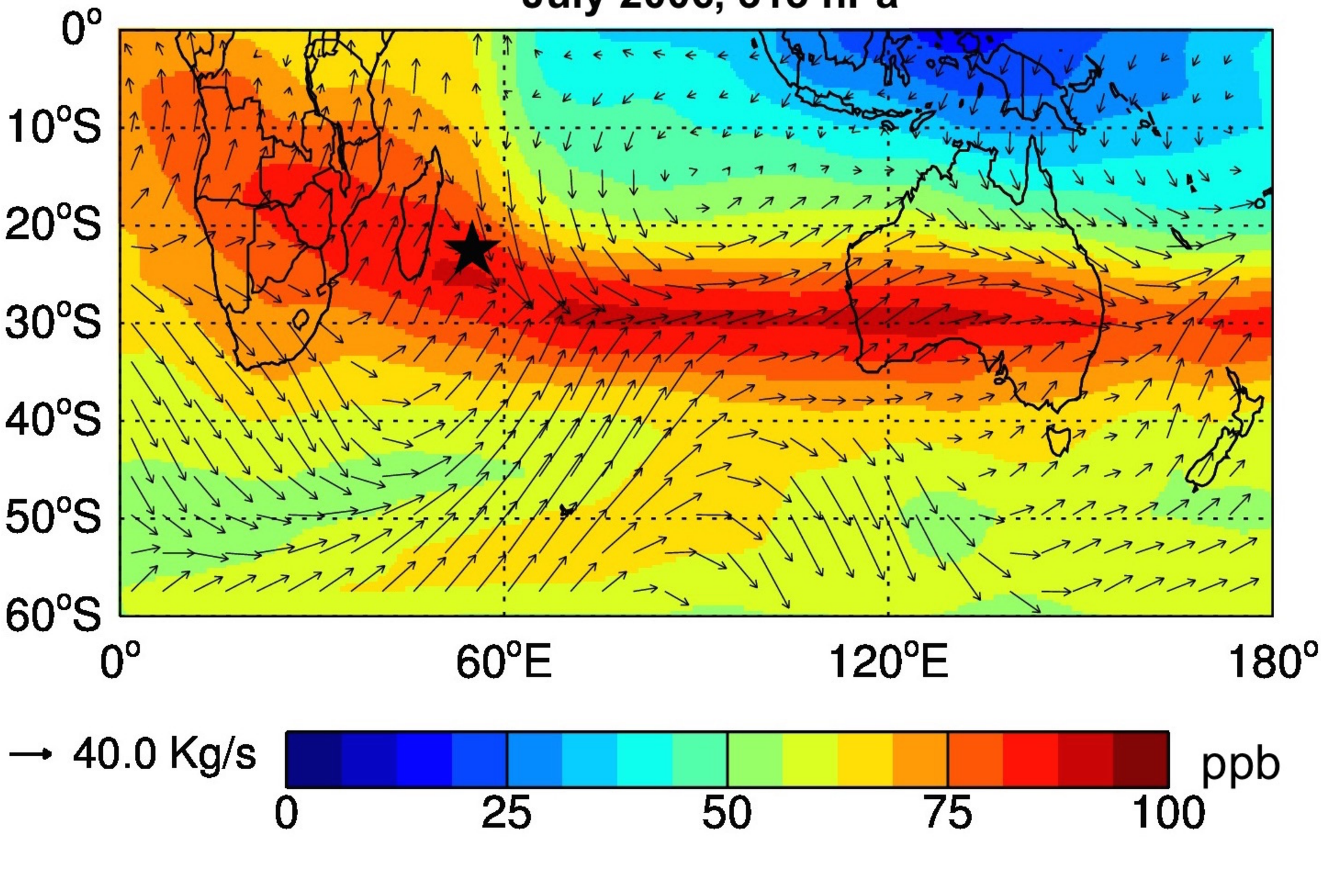

a) Réunion Sondes (1992-2014)

b) Hindcast-VE (2°x2.5°)

Pressure (hPa)

120
150
200
300
400
500
600
700

J F M A M J J A S O N D J J F M A M J J A S O N D J

18 18 19 19 18 18 17 18 19 19 19 21

# of mons

ppb/decade

-8 -6 -5 -3 -1 0 2 4 6 8 10 11 13 15 17 19 21 23 25

S. Africa (35S-6N, 8E-51E)

East (10S-40N, 70E-125E)

NO Total
NO FF
NO BB

0.007+- 0.006 July

0.069+- 0.005 July

0.007+- 0.010 August

0.058+- 0.014 August

0.027+- 0.011 September

0.054+- 0.028 September

NO emissions (kt/mon)

0 2 4 6

91 93 95 97 99 01 03 05 07 09 11

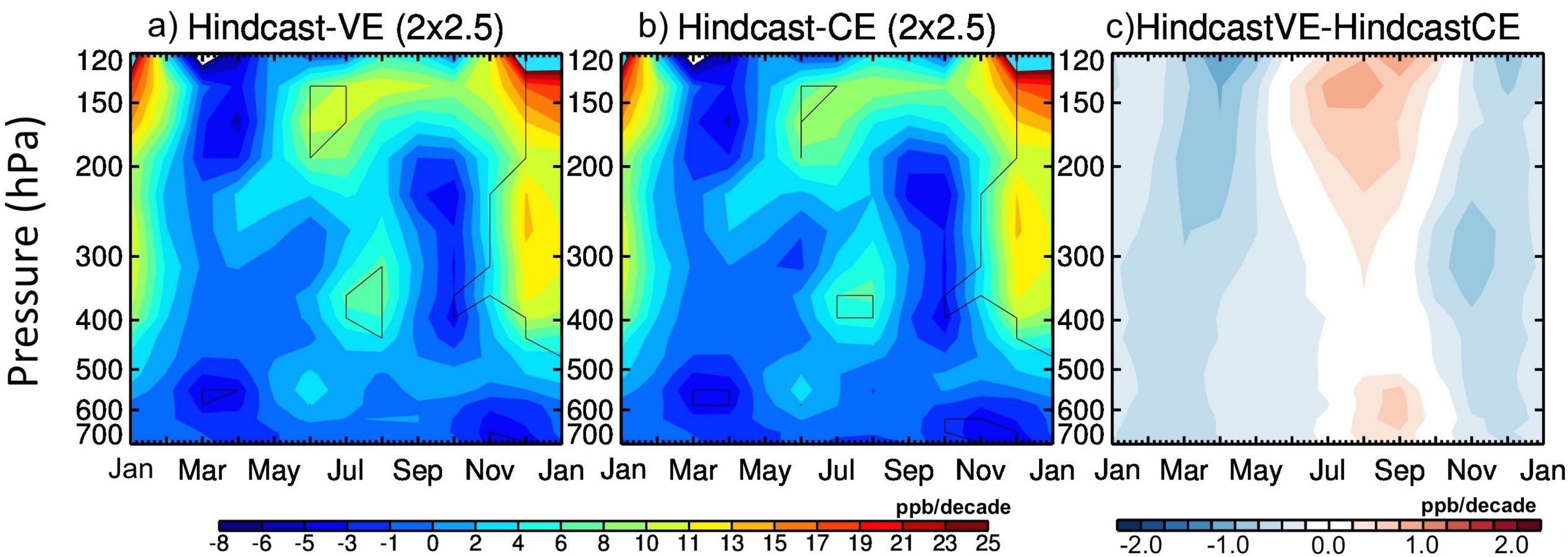
a) Hindcast-VE (2x2.5)
b) Hindcast-CE (2x2.5)
c)HindcastVE-HindcastCE
Pressure (hPa)
120
150
200
300
400
500
600
700
Jan Mar May Jul Sep Nov Jan
ppb/decade
-8 -6 -5 -3 -1 0 2 4 6 8 10 11 13 15 17 19 21 23 25
-2.0 -1.0 0.0 1.0 2.0